Journal of Hydraulic Research

ISSN: 0022-1686 (Print) 1814-2079 (Online) Journal homepage: http://www.tandfonline.com/loi/tjhr20

# Flow structure at a confluence: experimental data and the bluff body analogy

**Horacio S. Herrero, Carlos M. García, Francisco Pedocchi, Guillermo López, Ricardo N. Szupiany & Cecilia E. Pozzi-Piacenza**

**To cite this article:** Horacio S. Herrero, Carlos M. García, Francisco Pedocchi, Guillermo López, Ricardo N. Szupiany & Cecilia E. Pozzi-Piacenza (2016): Flow structure at a confluence: experimental data and the bluff body analogy, Journal of Hydraulic Research, DOI: 10.1080/00221686.2016.1146804

**To link to this article:** http://dx.doi.org/10.1080/00221686.2016.1146804

Published online: 11 Apr 2016.

*Journal of Hydraulic Research*, 2016
http://dx.doi.org/10.1080/00221686.2016.1146804




Research paper

# Flow structure at a confluence: experimental data and the bluff body analogy

HORACIO S. HERRERO, Assistant Professor, *Consejo Nacional de Investigaciones Científicas y Técnicas (CONICET), Centro de Estudios y Tecnología del Agua (CETA – UNC), Córdoba, Argentina*
*Email: hsherrero@yahoo.com.ar*

CARLOS M. GARCÍA, Associate Professor, *Consejo Nacional de Investigaciones Científicas y Técnicas (CONICET), Centro de Estudios y Tecnología del Agua (CETA – UNC), Córdoba, Argentina*
*Email: cgarcia2mjc@gmail.com (author for correspondence)*

FRANCISCO PEDOCCHI, Associate Professor, *Facultad de Ingeniería, Instituto de Mecánica de los Fluidos e Ingeniería Ambiental (IMFIA), Universidad de la República., Montevideo, Uruguay*
*Email: kiko@fing.edu.uy*

GUILLERMO LÓPEZ, Assistant Professor, *Facultad de Ingeniería, Instituto de Mecánica de los Fluidos e Ingeniería Ambiental (IMFIA), Universidad de la República., Julio Herrera y Reissig 565, Montevideo, CP 11300, Uruguay*
*Email: glopezmendez@gmail.com*

RICARDO N. SZUPIANY, Associate Professor, *Consejo Nacional de Investigaciones Científicas y Técnicas (CONICET), Centro Internacional de Estudios de Grandes Ríos (CIEGRI-UNL), Santa Fe, Argentina*
*Email: rszupiany@yahoo.com.ar*

CECILIA E. POZZI-PIACENZA, Associate Professor, *Centro de Estudios y Tecnología del Agua (CETA – UNC), Córdoba, Argentina*
*Email: cpozzi@efn.uncor.edu*

**ABSTRACT**
An experimental characterization of the hydrodynamics of a mixing interface at an open channel confluence is presented. In the laboratory experiments, both a confluence and a cylinder set-up were studied in order to validate the bluff body analogy, which has been proposed to characterize the mixing interface. The experimental characterization included flow visualization and the computation of the mean flow field, time scales of the coherent structures, and turbulent kinetic energy. The comparison among the two configurations confirms the validity of the analogy as similar features were found for the mean flow field and time scales of the coherent structures. However, differences in the length of the stagnation zone, the flow velocity deficit, and the turbulence intensity were observed. These differences should be taken into account when the bluff body analogy is used to characterize the confluence hydrodynamics and to quantify the mixing at the confluence interface.

*Keywords:* Acoustic Doppler techniques; coherent structures; laboratory studies; mixing process; river channels confluence; turbulent wakes; velocity measurements

## 1 Introduction

Stream confluences play an important role in the dynamics of fluvial systems as they regulate the movement of sediment through braided river systems. The confluence hydrodynamics are characterized by the presence of complex flow patterns (Boyer, Roy, & Best, 2006; Constantinescu, Miyawaki, Rhoads, Sukhodolov, & Kirkil, 2011), which are influenced by topographic effects induced by the presence of bed forms, large scale bed roughness, and large scale banks irregularities (Sukhodolov & Rhoads, 2001). An important feature of confluence hydrodynamics is the formation of a mixing interface

Received 6 November 2014; accepted 22 January 2016/Currently open for discussion.

ISSN 0022-1686 print/ISSN 1814-2079 online
http://www.tandfonline.com

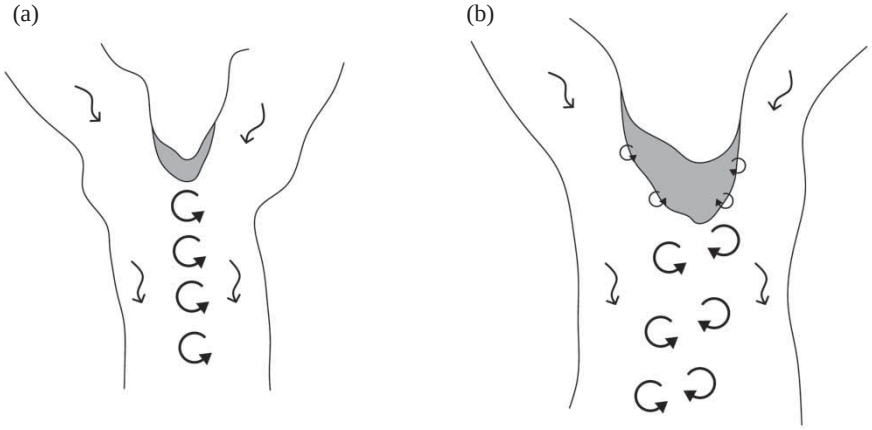


Figure 1 Hydrodynamic patterns observed at the mixing interface of river confluences: (a) Kelvin–Helmholtz (KH) features; and (b) turbulent wake (TW) features. The stagnation zone is shown in grey



between converging flows and the development of large scale coherent structures within this interfacial region. Mixing interfaces have been generally analysed in the near-field of mixing as a shallow shear layer, where lateral mass and momentum exchange are considered negligible (Constantinescu et al., 2011). However, in a small natural river confluence, Rhoads and Sukhodolov (2004) observed a stagnation zone with recirculating fluid at the junction apex, which was bounded on each side by smaller shear layers. The stagnation zone is one of the distinct elements of confluence hydraulics defined by Best (1987). At the downstream end of the stagnation zone, eddies from each of the two shear layers are alternately shed into the mixing interface to form larger quasi 2-D coherent structures. Constantinescu et al. (2011) claimed that, due to this alternate shedding, the mixing interface will include successive coherent structures rotating in opposite directions with alternating vorticity. In this case, the mechanism for formation of quasi 2-D eddies is similar to the vortex shedding process responsible of the development of coherent structures behind a bluff body.

Sukhodolov and Rhoads (2001) found through field observations, which were subsequently confirmed by Constantinescu, Miyawaki, Rhoads, and Sukhodolov (2012, 2014) and Constantinescu (2014) using numerical simulations, that the mixing interface will be dominated by either Kelvin–Helmholtz (KH) features or turbulent wake (TW) features depending on the planform geometry, the angle between the incoming flows and the flow velocity ratio across the mixing interface. In the first case, the mixing interface includes predominantly quasi two-dimensional large-scale co-rotating turbulence structures, whose growth is driven by KH instability and by vortex pairing. In the second case, the mixing interface includes quasi two-dimensional large-scale coherent turbulence structures with opposite directions of rotation. Both hydrodynamic patterns are shown in Fig. 1.

Constantinescu et al. (2012) claimed that in natural river confluences both hydrodynamic features (KH and TW) may be present simultaneously in the mixing interface but often one pattern will dominate over the other, with the dominant flow feature being determined by the flow conditions, the confluence geometry and morphology. Constantinescu et al. (2011) affirmed that KH features will dominate, when the converging flow momentum and velocities have different magnitudes. Meanwhile TW features will dominate when converging flow momentum and velocities have similar magnitudes.

Despite the mentioned numerical simulations, there is a clear need for experimental validation of the KH and TW analogies. According to Constantinescu et al. (2011), this additional research should be focused on river confluences in which other process affecting mixing, such as bedform presence or bank irregularities, are negligible. These controlled conditions can be easily achieved in the laboratory, using a simplified geometry and a constant flow rate. Quantification of the temporal and spatial variation of the mixing interface is important for the validation of numerical models used to quantify flow and mass transport in river confluences. In particular, it is important to quantify the relations among the turbulence kinetic energy (*TKE*), its dissipation rate, and the characteristic length scale of turbulent processes (Rhoads & Sukhodolov, 2008).

This paper presents new laboratory results obtained with the objective of characterizing the mixing interface hydrodynamics in an open channel confluence with a fixed concordant bed (no bed erosion is simulated) and with no density difference of the converging flows. In the experiments, the momentum and flow velocity ratios between the converging flows were set close to unity, to promote the development of wake-generated structures at the mixing interface. Then the experimental set-up was modified to observe the flow around a circular-cylindrical bluff body. This approach adopted theoretical considerations from fluid mechanics (i.e. TW behind a bluff body) to characterize the features of the mixing interface. The experimental characterization (for both confluence and bluff body experimental set-ups) includes flow visualization and the computation of the mean

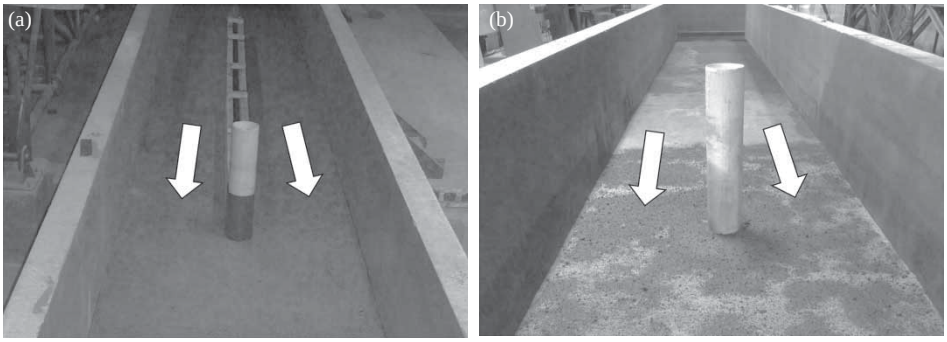


Figure 2 Experimental set-ups: (a) confluence; and (b) cylindrical bluff body



flow and turbulence intensities, *TKE*, as well as the temporal scales of the coherent structures.

## 2 Experimental set-up, method and instrumentation

The experiments described here were performed in a laboratory flume located in the Instituto de Mecánica de los Fluidos e Ingeneiría Ambiental, Facultad de Ingeniería, Universidad de la República, Montevideo, Uruguay. The flume is 18 m long and 1.5 m wide. A pumping system is composed by a pump (maximum flow discharge of 200 l s$^{-1}$) that takes water from a large reservoir, several control valves, and an ultrasound flowmeter. The flume bed was covered by a 0.25 m thick layer of uniform sand, with mean size 0.8 mm. The bed was flattened and fixed by spreading a very small amount of cement in the stagnation zone and mixing interface, before the beginning of the experiment. The water depth was controlled by a valve located at the downstream end of the flume. Two experimental set-ups have been used in this study (Fig. 2). One was employed to simulate parallel confluent flows with velocity ratio equal to 1, and the other flows around a cylindrical bluff body. The confluence apex width was the same as the diameter of the bluff body ($D = 0.16$ m), and was located 8 m downstream of the flume entrance.

Table 1 summarizes the tested flow conditions for each experimental set-up. The kinematic viscosity of the water was in all cases $\nu = 1 \times 10^{-6}$ m$^2$ s$^{-1}$. The experiments were designed so that the same bulk hydraulic parameters (i.e. mean cross sectional velocity and flow depth downstream of confluence/cylinder) were present for both set-up configurations. However, it should be noted that the effective width of the flume for the incoming flows was different, being 0.16 m narrower for the confluence set-up, as can be observed in Fig. 2. This resulted in the mean velocities of the incoming flows being 11% larger for the confluence set-up.

A qualitative characterization of the coherent structures in the mixing interface was achieved using two different dye-tracers (Methylene blue and Kaolinite) and a 12-megapixel digital camera Panasonic® (Newark, NJ, USA) model DMC-ZR1. The flow velocity was measured at several locations along the mixing interface (Fig. 3) and in the incoming flow zones using an

Table 1 Flow conditions analysed in this paper for both set-up configurations representing flow confluence and flow around a cylindrical bluff body

| | | Setup configuration | |
|---|---|---|---|
| Parameter | Unit | Confluence | Bluff body |
| Flow discharge ($Q$) | (l s$^{-1}$) | 80 | 80 |
| Water depth ($H$) | (m) | 0.26 | 0.26 |
| Effective width of incoming flows ($B$) | (m) | 1.34 | 1.50 |
| Mean velocity of incoming flow ($U_m = Q/Area$) | (m s$^{-1}$) | 0.23 | 0.21 |
| Reynolds number $\mathsf{R} = U_m\, H/\nu$ | – | $6.0 \times 10^4$ | $5.3 \times 10^4$ |
| Froude number $\mathsf{F} = U_m / (gH)^{0.5}$ | – | 0.14 | 0.13 |
| Obstacle Reynolds numbers = $\mathsf{R_D} = U_m\, D/\nu$ | – | $3.7 \times 10^4$ | $3.3 \times 10^4$ |

acoustic Doppler velocimeter (ADV) and ultrasonic velocimeter profiler (UVP). Time series of the three-dimensional flow velocity at several points downstream of the obstacle (Fig. 3) were recorded using a Vectrino 10 MHz ADV Lab with Plus firmware option® (Nortek, San Diego, CA, USA). These measuring points were all located at mid-depth $z = H/2$ for the two analysed set-ups, where $H$ is the flow depth. The ADV recording frequency was $f_R = 25$ Hz, which satisfies the condition $\mathsf{F_R} = f_R \cdot T_f > 20$ for accurate turbulence characterization (García, Cantero, Niño, & García, 2005). Here $T_f$ is the integral time scale of the flow turbulence, estimated as $T_f = L/U_{\text{conv}}$, $L$ is the largest turbulence length scale generated by bottom friction (on the order of the flow depth $H$) and $U_{\text{conv}}$ is the convective velocity of the turbulence structures (on the order of the mean flow velocity in the streamwise direction).

Velocity time series were also recorded along different locations downstream of the obstacle (Fig. 3) and in the incoming flow region using the UVP from Met-Flow (Lausanne, Switzerland). This instrument records the projection of the velocity vector along the axis of the acoustic beam emitted by the sensor (more details can be found in Pedocchi & Garcia, 2009). Vertical profiles of streamwise and vertical flow velocity components were recorded 1 m upstream of the confluence apex and the

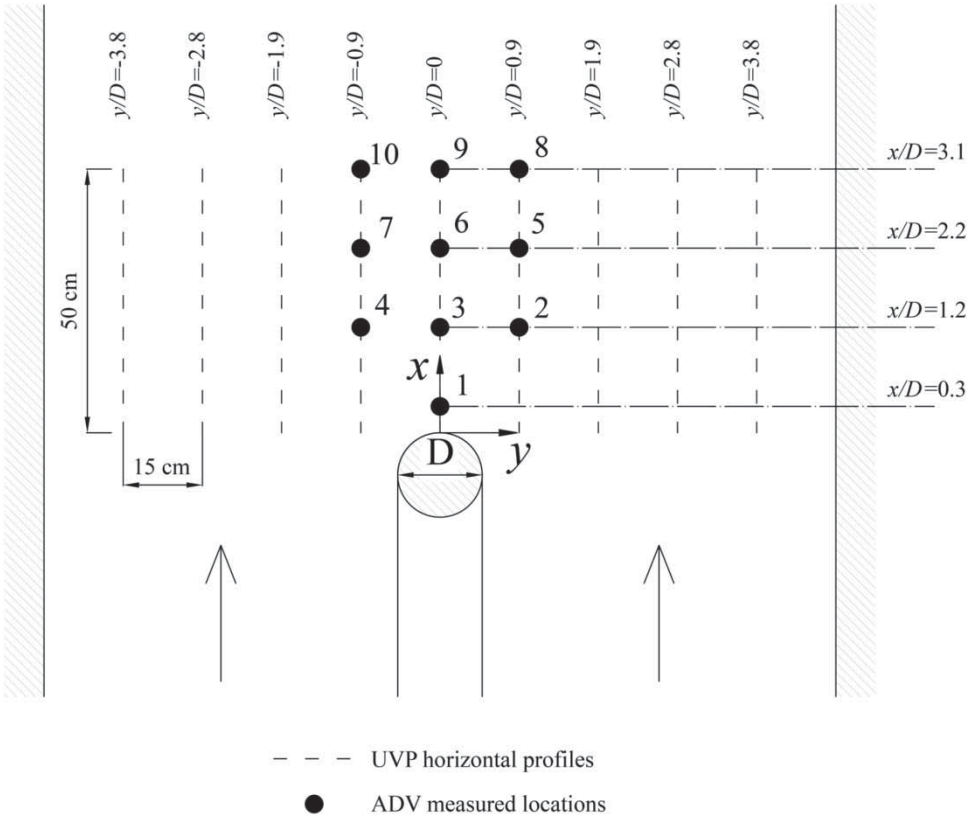


Figure 3 Locations of ADV and UVP velocity measurements downstream of the obstacle or confluence apex ($x$ and $y$ represent the streamwise and transverse directions, respectively)

obstacle with three 4 MHz UVP sensors (one vertical and two at 30° angle), with a sampling frequency of 40 Hz, for 410 s. The vertical profiles were measured over three streamwise planes, located 0.3 m from each wall and on the centreline of the flume, the centreline measurements were not obtained for the confluence configuration due to the presence of the splitter plate. Nine horizontal profiles of the streamwise velocity component were recorded along 0.5 m horizontal segments downstream from the confluence apex/cylinder. These segments were located at mid-depth $z = H/2$ from the channel bed. The velocity was measured using 2 MHz UVP sensors running at a sampling frequency of 25 Hz, for 328 s.

## 3 Results

### 3.1 *Characterization of incoming flows*

Figure 4 shows the dimensionless profiles of the streamwise velocity recorded with the UVP 1 m upstream from the confluence apex/cylinder. The shear velocity $u_*$ was computed from fitting the log-law to the data (Nezu, 1993); the results are summarized in Table 2. No sediment motion was observed during the experiments assuring clear water conditions in the upstream region. This was in agreement with the fact that the $u_*/u_{*\text{critical}}$ was always below one, where $u_{*\text{critical}}$ was computed from the Shields diagram ($u_{*\text{critical}} = 1.46\,\text{cm}\,\text{s}^{-1}$, Garcia, 2008).

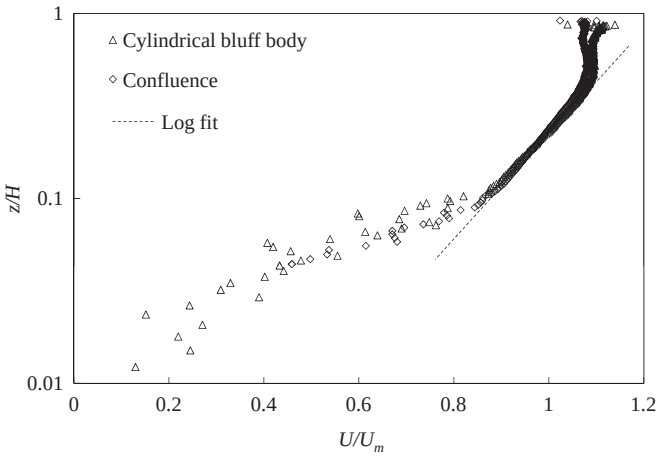


Figure 4 Dimensionless mean streamwise velocity profiles measured 1 m upstream of the mixing interface for both set-up configurations (representing flow confluence and flow around cylindrical bluff body). The velocity profiles were recorded at the centreline of the right channel for the confluence configuration and in the centreline of the whole channel for the flow around cylindrical bluff body

### 3.2 *Visualization of flow features in the mixing interface of the flow confluence*

Figure 5 shows the results of the flow visualization along the mixing interface for the confluence set-up. During the experiment the dye-tracers were injected to the incoming flows on each side of the confluence. Quasi 2-D coherent structures can

Table 2 Shear velocities ($u_*$) computed for the incoming flow for both set-up configurations representing flow confluence and flow around cylindrical bluff body ($Q = 80\,\mathrm{l\,s^{-1}}$). Values of the critical shear velocities ($u_{*\mathrm{critical}}$) for sediment motion are also shown

| Setup configuration | Location | $u_*$ (cm s$^{-1}$) | $u_{*\mathrm{critical}}$ (cm s$^{-1}$) | $u_*/u_{*\mathrm{critical}}$ (%) |
|---|---|---|---|---|
| Cylindrical bluff body | Centreline | 1.09 | 1.46 | 75 |
| Confluence | Left channel | 1.21 | 1.46 | 83 |
| | Right channel | 1.24 | 1.46 | 85 |

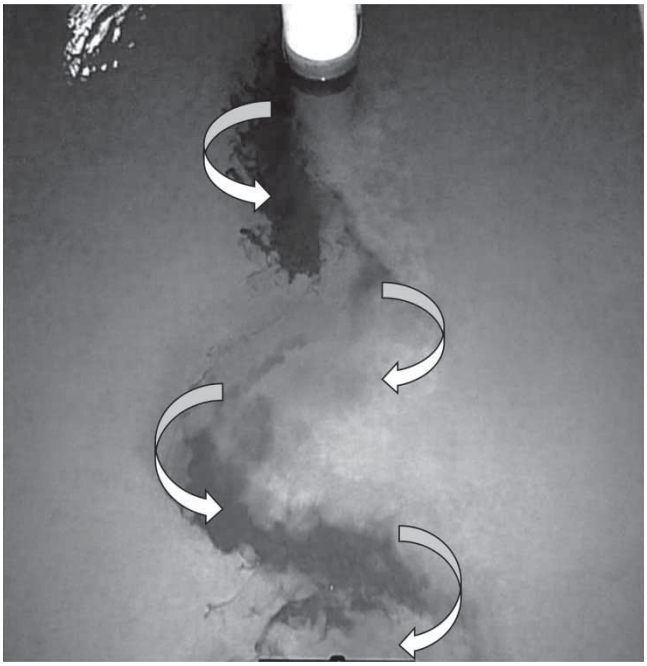

Figure 5 Visualization (using tracers) of coherent structures at the mixing interface of the confluence experimental configuration

be observed at the downstream end of the stagnation zone shedding alternately into the mixing region. These coherent structures are similar to the ones reported by Rhoads and Sukhodolov (2004) in a small river confluence. Rhoads and Sukhodolov (2004) claim that the process of eddy development appears to be similar to traditional vortex pairing, where small individual vortices with vertical axis of rotation, moving at different speeds on each side of the shear layer, amalgamate as they move in the downstream direction to produce large coherent structures.

On Fig. 5 coherent structures with opposite direction of rotation are observed, similar to those simulated by Constantinescu et al. (2011) and Constantinescu et al. (2012) in angled confluences with momentum ratio near 1. These coherent structures are analogous to those observed along the wake behind a cylindrical bluff body (Chen & Jirka, 1995), agreeing with the conceptual model proposed by Sukhodolov and Rhoads (2001), Fig. 2b.

### 3.3 *Mean flow velocity field in the mixing interface*

To quantify the similarity among the hydrodynamic features in the mixing interface for the case of the flow in a confluence and around a cylindrical bluff body, the mean velocity fields are compared. Figure 6a shows the mean streamwise flow velocity fields obtained from the UVP horizontal profiles downstream of the obstacle for both set-up configurations while Fig. 6b shows the dimensionless mean streamwise velocities for both set-ups.

Figure 6a and b shows that for both configurations a streamwise velocity deficit (including a stagnation zone) develops in the lee of the splitter plate (confluence configuration) and cylinder (bluff-body configuration). For the bluff body set-up the streamwise velocities on the sides of the obstacle are greater than for the confluence set-up. This is due to the accelerations imposed on the flow passing around the obstacle. In addition, the flow velocity deficit is larger for the cylindrical bluff body set-up. Mean streamwise velocity $U_{ij}$ obtained at each location "$i$" along the streamwise direction $x$, and "$j$" along the transverse direction $y$, are made dimensionless using the mean velocity of incoming flow $U_m$ (Table 1). Figure 6b shows the dimensionless mean streamwise velocities for both set-ups. The coordinates were also made dimensionless using the diameter of the confluence apex and the cylindrical bluff body diameter ($D = 0.16\,\mathrm{m}$, the same for both set-ups).

The spatial evolution of mean streamwise flow velocity recorded using UVP in the centreline of the mixing interface is plotted in Fig. 7, for both set-ups; experimental results from Lourenco and Shih (1993) for a flow around a cylindrical bluff body are also included. The results for the cylindrical bluff body set-up are in good agreement with the data of these authors.

The velocity deficit region for both set-ups includes the stagnation zone where negative (or zero) streamwise mean velocity values are observed (Fig. 7). The negative values are related to the existence of recirculating cells behind the obstacle. For cylindrical bluff body configuration, the stagnation zone extends over a distance of $1.8D$ with a minimum mean streamwise velocity of $-0.3U_m$ downstream, while for the confluence set-up the extension of the stagnation zone is $1.4D$ with a minimum mean streamwise velocity of $-0.17U_m$. Furthermore $2.5D$ downstream similar values are observed for the streamwise mean velocity for both set-ups.

### 3.4 *Spatial evolution of flow fluctuations intensity in the mixing interface*

The downstream evolution of the flow fluctuation intensities is analysed using values of the root mean square ($RMS_x$) of the streamwise velocity signal recorded with the UVP for both set-ups (Fig. 8).

High values of $RMS_x$ were obtained along the mixing interface downstream from the obstacle for both set-ups. This

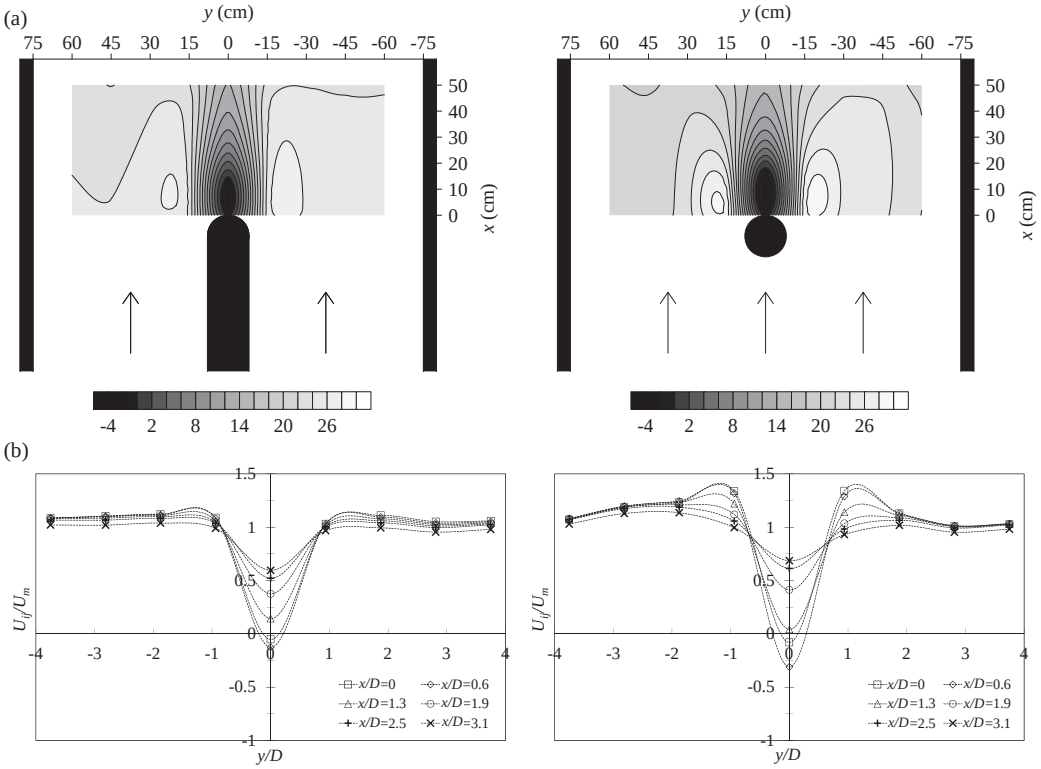


Figure 6 (a) Mean streamwise flow velocity fields (cm $s^{-1}$); and (b) transverse profiles of dimensionless mean streamwise flow velocity obtained using UVP downstream of the confluence apex (left) and cylindrical bluff body (right)

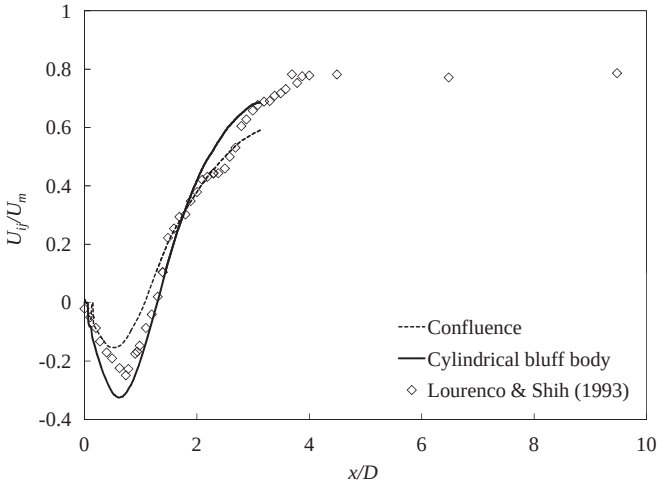


Figure 7 Spatial evolution of dimensionless mean streamwise flow velocity in the centreline of the channel recorded using UVP, and experimental results obtained by Lourenco and Shih (1993)

increase in $RMS_x$ is clearly due to the presence of the coherent flow structures shedding from the obstacle. Although similar patterns of dimensionless $RMS_x$ values were observed for both set-ups, the cylindrical bluff body configuration has larger values of $RMS_x$ than those for the confluence configuration. In addition, Fig. 8 shows that the width of the region of large $RMS_x$ values is greatest for the cylindrical bluff body set-up. The evolution of dimensionless $RMS_x$ along the cross section at $x = 2.5D$ and $x = 3.1D$ downstream of the obstacle is shown in Fig. 9 for both set-ups.

For the confluence set-up, the region with high values of $RMS_x$ covers a distance of about $1D$ on each side of the centreline with a maximum $RMS_x$ of $0.16U_m$. For the cylindrical bluff body set-up high values of $RMS_x$ exists up to $2D$ on each side of the centreline with a maximum $RMS_x$ of $0.26U_m$. A deficit in the peak values of $RMS_x$ at a streamwise distance of $x/D > 3$ is evident for the cylindrical bluff body set-up in agreement with previous results by Kravchenko and Moin (2000).

### 3.5 *Temporal time scales of coherent structures in the mixing interface*

The temporal time scale of the turbulent structures observed along the mixing interface was estimated through spectral analysis of the recorded velocities for both experimental set-ups. First, the spectral density functions were computed for the 3D velocity recorded with the ADV. Note that the Doppler noise energy has been subtracted for the spectra presented on Figs 11 and 10, following García et al. (2005).

#### 3.5.1 *Spectral analysis for locations in the mixing interface at the centreline of the channel (y/D = 0)*

Spectral density function for the transverse velocity component (Fig. 11) at the centreline of the channel ($y/D = 0$) presents a peak at frequencies ranging between 0.27 and 0.3 Hz (Table 3) for both set-up configurations, and the maximum energy peaks were observed at the centreline a distance $x = 1.2D$ downstream of the obstacle, being 12,814 $cm^2\ s^{-1}$, and 351 $cm^2\ s^{-1}$ for the

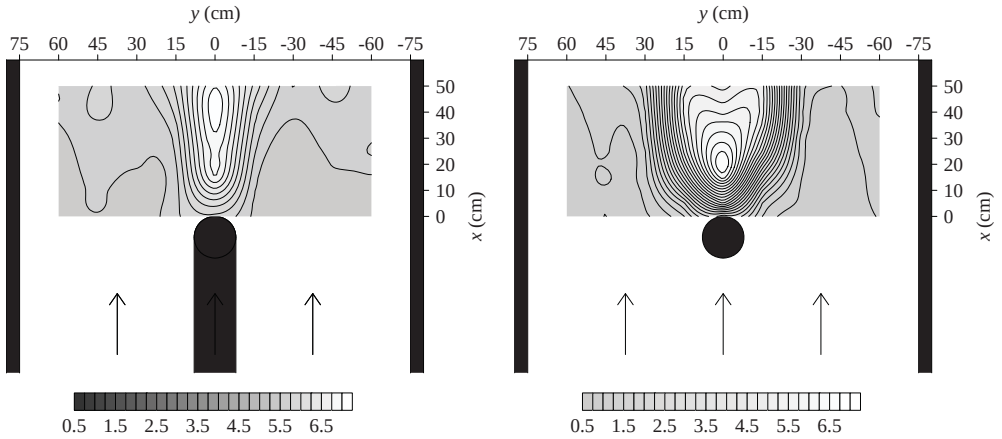


Figure 8 $RMS_x$ values (cm $s^{-1}$) for the streamwise flow velocity signals recorded using a horizontal UVP downstream of the obstacle, for flow confluence (left) and flow around cylindrical bluff body (right) configuration set-ups

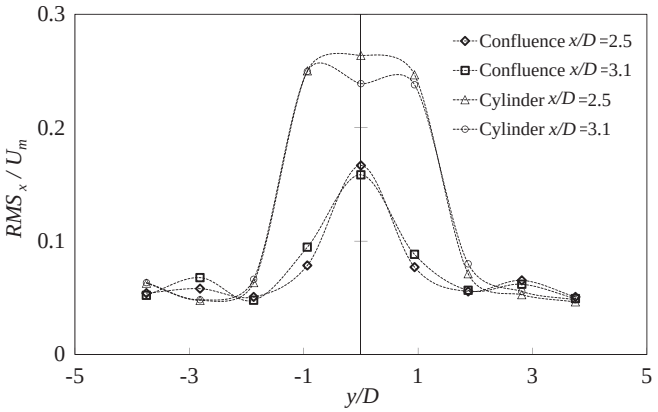


Figure 9 Dimensionless $RMS_x$ of streamwise flow velocity signal recorded in the mixing interface downstream of the obstacle

cylindrical bluff body and flow confluence set-up, respectively. For the streamwise and vertical velocity components, a clear peak on the spectral density functions is not observed at the centreline (Fig. 11).

### 3.5.2 *Spectral analysis for points located at y/D = 0.9*

Power spectra for the transverse and streamwise velocity components (Fig. 10) at $y/D = 0.9$ also show a peak at frequencies ranging between 0.27 and 0.3 Hz. The vertical velocity component does not exhibit a pronounced peak (Fig. 10) at $y/D = 0.9$ and different streamwise locations. For the confluence set-up, the maximum spectral peaks for the transverse and streamwise velocity components at ($y/D = 0.9$) are equal to 63 $cm^2\ s^{-1}$ and 59 $cm^2\ s^{-1}$, respectively, while for the cylindrical bluff body set-up, the energy peaks for the transverse and streamwise velocities were equal to 1755 $cm^2\ s^{-1}$ and 1082 $cm^2\ s^{-1}$, respectively.

## 3.6 *Frequency analysis of coherent structures shedding*

The frequency of the observed peaks in the spectral density functions is directly related to the vortex shedding frequency, through the Strouhal number S. This dimensionless number includes the shedding frequency of the coherent structures $f$, a characteristic length (in this case the diameter of the cylindrical bluff body or the confluence apex width $D$) and a characteristic flow velocity (in this case the mean velocity of the approaching flow $U_m$), then $S = fD/U_m$.

Previous results by Schewe (1983) showed that the Strouhal number of the flow around a cylindrical bluff body increases as the obstacle Reynolds number $R_D$ increases, reaching an approximately constant value of $S \approx 0.2$ for $R_D$ between 300 and $3 \times 10^5$. Experiments reported here have $R_D \approx 3 \times 10^4$, falling in the constant Strouhal number range. Table 3 shows the Strouhal numbers computed for the streamwise and transverse velocity components measured with ADV at different locations (Fig. 3) for the cylindrical bluff body and confluence set-up. The observed Strouhal numbers are in good agreement with previous studies. Table 3 does not include Strouhal number for the streamwise flow velocity component recorded at the centreline (locations 1, 3, 6 and 9) because there were no noticeable peaks in the spectral density function, and therefore $f$ was not clearly defined.

For all the sampled locations, the Strouhal number values obtained in the mixing interface of the confluence set-up showed good agreement with the empirical value of 0.2 predicted for a bluff body configuration. These results agree with Rhoads and Sukhodolov (2008), who reported a Strouhal number of 0.2 for coherent structures in the mixing interface at a small natural confluence.

## 3.7 *Fluctuating kinetic energy per unit mass*

The average fluctuating kinetic energy per unit mass $K$, computed as:

$$K = \frac{1}{2}[u'^2 + v'^2 + w'^2], \quad (1)$$

where $u'^2$, $v'^2$ and $w'^2$ are the variances (including noise correction) of the recorded velocity signal for each Cartesian

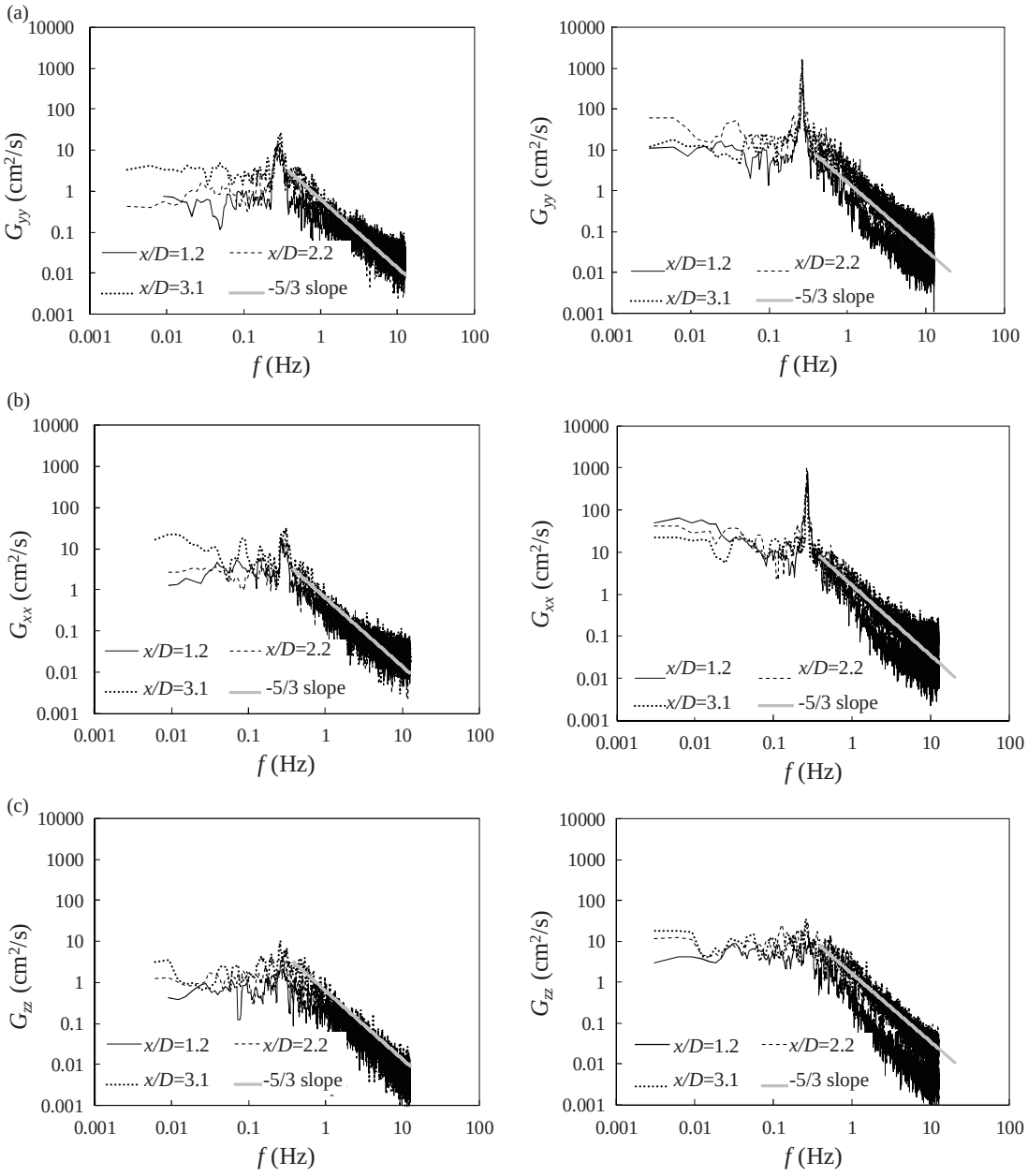


Figure 10 Spectral density functions of: (a) transverse ($G_{yy}$), (b) streamwise ($G_{xx}$), and (c) vertical ($G_{zz}$) flow velocity components measured with ADV at different streamwise locations at $y/D = 0.9$ for confluence (left) and cylindrical bluff body (right) experimental set-ups. The figures include the $-5/3$ power law fitting

component, including flow fluctuation contributions from different processes (i.e. approach turbulence, coherent structures shedding, etc.). The fluctuating kinetic energy contribution from flow turbulence is usually referred to as *TKE* (turbulent kinetic energy). Table 4 shows values of *K* and *TKE* computed from velocity signals measured with ADV at different locations for both set-ups, at progressives $x > D$ (locations 2 to 10).

The turbulent kinetic energy *TKE* values were estimated using the variances of the high pass filtered flow velocity signals. A Fourier high-pass filter was implemented with a cut-off frequency of 0.5 Hz, which is larger than the frequency of coherent structures shedding (between 0.27 and 0.3 Hz). The variance contribution of the flat plateau of the spectrum for the smallest frequencies has been considered.

Both the *K* and *TKE* values are considerably larger in the cylindrical bluff body experimental set-up than the confluence set-up due to the more intense shedding of coherent structures and turbulence for this set-up. However, it should be noticed that *TKE* / *K* ratios are similar for both set-ups. This shows that both the shedding of coherent structures and the turbulence generation are strongly related, having the same origin in the detachment of the boundary layer around the cylinder or the confluence apex.

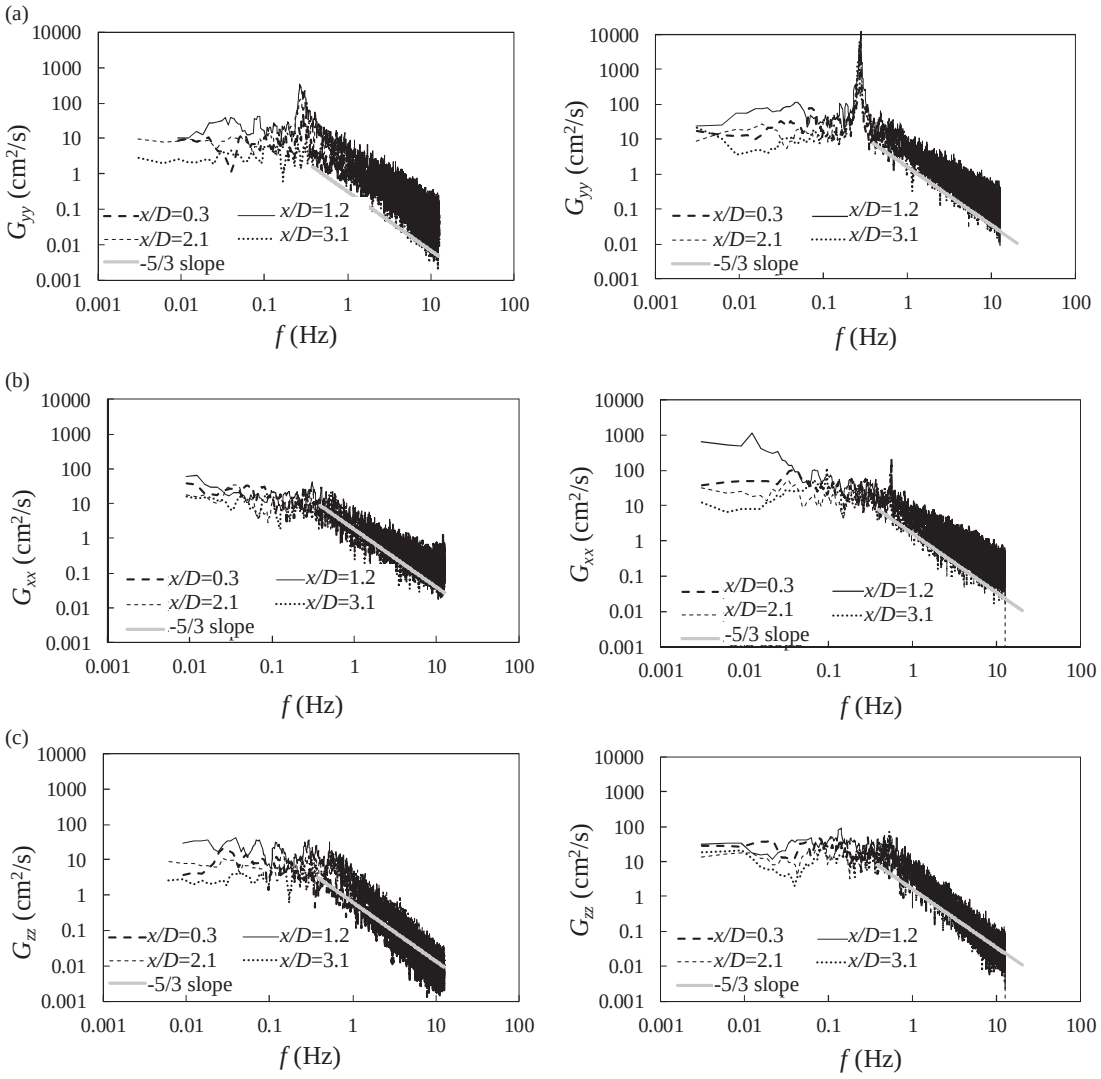


Figure 11 Spectral density functions of: (a) transverse ($G_{yy}$), (b) streamwise ($G_{xx}$), and (c) vertical ($G_{zz}$) flow velocity components measured with ADV at different locations along the centreline of the mixing interface for confluence (left) and cylindrical bluff body (right) experimental set-ups. The figures include the − 5/3 power law fitting

Table 3 Frequency of the observed peaks in the spectral density functions ($f$) and Strouhal number (S) computed for the streamwise and transverse velocity components measured with ADV at different locations for confluence and flow around a cylindrical bluff body configuration set-ups

| | Confluence | | | | Bluff body | | | |
|---|---|---|---|---|---|---|---|---|
| | Streamwise component | | Transversal component | | Streamwise component | | Transversal component | |
| Location | $f$ (Hz) | S | $f$ (Hz) | S | $f$ (Hz) | S | $f$ (Hz) | S |
| 1 | – | – | 0.278 | 0.22 | – | – | 0.284 | 0.22 |
| 2 | 0.272 | 0.21 | 0.272 | 0.21 | 0.269 | 0.21 | 0.269 | 0.21 |
| 3 | – | – | 0.275 | 0.21 | – | – | 0.262 | 0.20 |
| 4 | 0.275 | 0.21 | 0.275 | 0.21 | 0.281 | 0.22 | 0.275 | 0.21 |
| 5 | 0.262 | 0.20 | 0.262 | 0.20 | 0.299 | 0.23 | 0.317 | 0.25 |
| 6 | – | – | 0.275 | 0.21 | – | – | 0.327 | 0.25 |
| 7 | 0.269 | 0.21 | 0.269 | 0.21 | 0.299 | 0.23 | 0.299 | 0.23 |
| 8 | 0.266 | 0.21 | 0.266 | 0.21 | 0.308 | 0.24 | 0.308 | 0.24 |
| 9 | – | – | 0.266 | 0.21 | – | – | 0.262 | 0.20 |
| 10 | 0.269 | 0.21 | 0.269 | 0.21 | 0.262 | 0.20 | 0.296 | 0.23 |

Table 4 Fluctuating kinetic energy ($K$) and turbulent kinetic energy ($TKE$) computed from velocity signals measured with ADV at different locations for confluence and cylindrical bluff body configuration set-ups

| | Confluence | | | Cylindrical bluff body | | |
|---|---|---|---|---|---|---|
| Location | $K$ (cm$^2$ s$^{-2}$) | $TKE$ (cm$^2$ s$^{-2}$) | $TKE/K$ | $K$ (cm$^2$ s$^{-2}$) | $TKE$ (cm$^2$ s$^{-2}$) | $TKE/K$ |
| 2 | 2.8 | 2.2 | 0.81 | 15.3 | 11.7 | 0.76 |
| 3 | 34.1 | 31.8 | 0.93 | 113.8 | 101.6 | 0.89 |
| 4 | 1.5 | 1.2 | 0.80 | 16.6 | 10.2 | 0.61 |
| 5 | 3.2 | 2.3 | 0.72 | 33.6 | 23.8 | 0.71 |
| 6 | 21.9 | 17.7 | 0.81 | 62.8 | 32.6 | 0.52 |
| 7 | 3.0 | 2.0 | 0.65 | 39.0 | 26.8 | 0.69 |
| 8 | 5.9 | 6.0 | 1.00 | 26.6 | 17.1 | 0.64 |
| 9 | 15.0 | 12.6 | 0.84 | 44.6 | 27.4 | 0.61 |
| 10 | 4.4 | 3.5 | 0.80 | 48.7 | 16.6 | 0.34 |



## 4 Conclusions

This paper presented an experimental characterization of the mixing interface of the flow in a confluence with parallel incoming flows and around a cylindrical bluff body. The detailed measurements provide important information towards validation of the analogy from fluid mechanics (i.e. TW behind a bluff body) that has been proposed to characterize the mixing interface.

While similar hydrodynamic patterns were observed in the case of the confluence and bluff body set-ups, the results also showed some differences that have been quantified. TW patterns were observed for both set-ups. First, the use of flow visualization techniques in the confluence set-up showed the presence of coherent structures downstream from the stagnation zone. These quasi 2-D coherent structures alternately shed into the mixing interface rotating in opposite directions similar to the ones observed in the wake of a cylindrical bluff body. Velocity measurements showed that for both experimental set-ups a velocity deficit is observed at the centreline of the mixing interface. This deficit is larger for the flow around a cylindrical bluff body and the stagnation zone extends further downstream in this configuration. In addition, due to the flow acceleration around the obstacle, the streamwise velocities just downstream of the sides of the cylindrical bluff body are larger than the ones observed in the case of the confluence.

This work also presents a spatial analysis of flow fluctuation intensity and a spectral analysis of the velocity signals for both configuration set-ups. Large values of dimensionless flow fluctuation intensity were observed for both set-ups. However, the flow around the cylindrical bluff body presented larger values of fluctuation intensity in the centreline due to more energetic coherent flow structures. Also, the flow around the cylindrical bluff body presented larger values of fluctuation intensity in the centreline due to more energetic coherent flow structures.

Temporal time scales of coherent structures within the mixing interface were computed through spectral analysis of the velocity signals recorded in both experimental set-ups. Similar fluctuations frequencies were observed for the transverse and streamwise velocities (not for vertical component). These results indicate that coherent structures are two dimensional with a vertical rotation axis. The Strouhal numbers computed for streamwise and transverse velocity components for flow around a cylindrical bluff body are in good agreement with previous studies ($S \approx 0.2$). In agreement with previous works (Rhoads & Sukhodolov, 2008), similar Strouhal numbers were observed for the confluence set-up, showing that the ratio between the approaching velocity and the diameter of the confluence apex are useful scales to characterize the vortex shedding frequency in a confluence.

The analysis of the different sources contributing to the fluctuating kinetic energy $K$ (turbulence and coherent structures shedding) provided support for the wake analogy. The $K$ values (including all the fluctuation contributions) at all the measured locations are considerably larger for the bluff body than for the confluence set-up. This is due to a more intense coherent structures shedding process. However, $TKE/K$ ratios are similar for both set-ups.

Highly similar hydrodynamics patterns were observed in the case of the confluence of parallel incoming flows and bluff body set-ups, confirming the validity of the wake analogy. However the results are not identical since some differences have been observed for similar flow conditions, especially related to the length of stagnation zone, the flow velocity deficit and the intensities of flow fluctuations generated by coherent structures.

It must be noted that the results of this study are limited for confluences of parallel incoming flows and the development of the stagnation zone is strongly influenced by flows converging at an angle. The enlargement of the stagnation zones at angled natural confluences and momentum ratios near 1 leads to more intense wake effects producing strong vortex shedding. This aspect of confluence hydrodynamics requires further investigation.

**Funding**

This work was supported by the Association of Universities Grupo Montevideo and the National Research and Innovation Agency (ANII) of Uruguay: Project ANII-Fondo María Viñas [PR_FMV_2009_1_3093].

**Notation**

$B$ = effective width of incoming flows (m)
$D$ = confluence apex width = diameter of the bluff body (m)
F = Froude number
$f$ = shedding frequency of the coherent structures estimated as the frequency of the observed peaks in the spectral density functions (Hz)
$F_R$ = dimensionless ADV recording frequency
$f_R$ = ADV recording frequency (m)
$G_{yy}, G_{xx}, G_{zz}$ = Spectral density functions of transverse, streamwise, and vertical velocity components, respectively
$H$ = flow depth (m)
$K$ = average fluctuating kinetic energy per unit mass ($cm^2\ s^{-2}$)
$L$ = largest turbulence length scale generated by bottom friction (m)
$Q$ = flow discharge ($l\ s^{-1}$)
R = Reynolds number
$R_D$ = obstacle Reynolds number
$RMS_x$ = root mean square of the streamwise velocity signal ($cm\ s^{-1}$)
S = Strouhal number
$T_f$ = integral time scale of the flow turbulence (s)
$TKE$ = turbulent kinetic energy ($cm^2\ s^{-2}$)
$u_*$ = shear velocity ($cm\ s^{-1}$)
$u_{*critical}$ = critical shear velocity for sediment motion ($cm\ s^{-1}$)
$U_{conv}$ = convective velocity of the turbulence structures ($m\ s^{-1}$)
$U_{ij}$ = mean streamwise velocity values measured at each location "$i$" along the streamwise direction $x$, and "$j$" along the transverse direction $y$ ($cm\ s^{-1}$)
$U_m$ = mean velocity of incoming flow ($m\ s^{-1}$)
$u'^2, v'^2, w'^2$ = variances (including noise correction) of the recorded velocity signal for each Cartesian component ($cm^2\ s^{-2}$)
$x, y, z$ = Cartesian coordinates (cm)
$\nu$ = kinematic viscosity of the water ($m^2\ s^{-1}$)

**References**

Best, J. L. (1987). Flow dynamics at river channel confluences: Implications for sediment transport and bed morphology.

Boyer, C., Roy, A. G., & Best, J. L. (2006). Dynamics of a river channel confluence with discordant beds: Flow turbulence, bed load sediment transport, and bed morphology. *Journal of Geophysical Research: Earth Surface*, *111*(F04007). DOI:10.1029/2005JF000458

Chen, D., & Jirka, G. H. (1995). Experimental study of plane turbulent wakes in a shallow water layer. *Fluid Dynamics Research*, *16*(1), 11–41.

Constantinescu, G. (2014). LE of shallow mixing interfaces: A review. *Environmental Fluid Mechanics*, *14*(5), 971–996.

Constantinescu, G., Miyawaki, S., Rhoads, B., & Sukhodolov, A. (2012). Numerical analysis of the effect of momentum ratio on the dynamics and sediment-entrainment capacity of coherent flow structures at a stream confluence. *Journal of Geophysical Research: Earth Surface*, *117*(F04028). DOI:10.1029/2012JF002452

Constantinescu, G., Miyawaki, S., Rhoads, B., & Sukhodolov, A. (2014). Numerical evaluation of the effects of planform geometry and inflow conditions on flow, turbulence structure, and bed shear velocity at a stream confluence with a concordant bed. *Journal of Geophysical Research: Earth Surface*, *119*(10), 2079–2097.

Constantinescu, G., Miyawaki, S., Rhoads, B., Sukhodolov, A., & Kirkil, G. (2011). Structure of turbulent flow at a river confluence with momentum and velocity ratios close to 1: Insight provided by an eddy-resolving numerical simulation. *Water Resources Research*, *47*(5), W05507. DOI:10.1029/2010WR010018

García, C. M., Cantero, M. I., Niño, Y., & García, M. H. (2005). Turbulence measurements with acoustic Doppler velocimeters. *Journal of Hydraulic Engineering*, *131*(12), 1062–1073.

Garcia, M. H. (2008), Sediment transport and morphodynamics. In M. H. Garcia (Ed.), Sedimentation engineering: Processes, measurements, modelling and practice (Chap. 2, pp. 21–164). Reston, Va: ASCE.

Kravchenko, A. G., & Moin, P. (2000). Numerical studies of flow over a circular cylinder at Re[sub D] = 3900. *Physics of Fluids*, *12*(2), 403–417.

Lourenco, L. M., & Shih, C. (1993). Characteristics of the plane turbulent near wake of a circular cylinder. A particle image velocimetry study. Private communication (data taken from Beaudan and Moin).

Nezu, I. (1993). *Turbulence in open-channel flows*. Rotterdam: A. A. Balkema.

Pedocchi, F., & Garcia, M. H. (2009). Application of an ultrasonic velocity profiler for velocity and suspended sediment measurements in an oscillatory boundary layer. Rep. 83, Civil Engineering Studies: *Hydraulic Engineering Series*, 53.UIUC. USA.

Rhoads, B. L., & Sukhodolov, A. N. (2004). Spatial and temporal structure of shear layer turbulence at a stream confluence. *Water Resources Research*, *40*(6), W06304. DOI:10.1029/2003WR002811

Rhoads, B. L., & Sukhodolov, A. N. (2008). Lateral momentum flux and the spatial evolution of flow within a confluence mixing interface. *Water Resources Research*, *44*(8), W08440. DOI:10.1029/2007WR006634

Schewe, G. (1983). On the force fluctuations acting on a circular cylinder in crossflow from subcritical up to transcritical Reynolds numbers. *Journal of Fluid Mechanics*, *133*, 265–285.

Sukhodolov, A. N., & Rhoads, B. L. (2001). Field investigation of three-dimensional flow structure at stream confluences: 2. Turbulence. *Water Resources Research*, *37*(9), 2411–2424.